



Facile Synthesis of La-modified CeO₂ with Microwave Method for CO₂ Adsorption

Svetlana A. Kuznetsova¹ · Olga S. Khalipova¹ · Alexandra G. Malchik² · Yu-Wen Chen³

Received: 3 October 2023 / Revised: 13 November 2023 / Accepted: 22 November 2023 / Published online: 15 February 2024
© The Author(s), under exclusive licence to Korean Institute of Chemical Engineers, Seoul, Korea 2024

Abstract

CO₂ capture in air is an important issue nowadays. Cerium oxide has been reported to be a good adsorbent for CO₂. However, its adsorption capacity and adsorption strength are not high enough. La-modified CeO₂ was used in this study. In this study: a new adsorbent La-modified CeO₂ solid solution were prepared from aqueous solution of cerium and lanthanum hydroxides by microwave method. These hydroxides were prepared by precipitation of Ce(NO₃)₃ and La(NO₃)₃ solution. The materials were characterized by powder X-ray diffraction, energy dispersive X-ray spectroscopic, scanning electron microscopy, infrared spectroscopy, and nitrogen sorption. The results show that the increasing the lanthanum content leads to a reduction in particle size, and increase in the number of oxygen vacancies in the crystalline structure and the specific BET surface areas of the samples. The La-CeO₂ materials contained impurities of nitrate ions in their structure and exhibited high adsorption properties for carbon dioxide at room temperature. The adsorption of carbon dioxide on the materials were in the form of bidentate. La-modified CeO₂ has large amount of CO₂ adsorption compared to the unmodified one.

Keywords Carbon capture · CO₂ adsorbent · Cerium oxide · Lanthanum oxide · Zero carbon emission · Microwave method

Introduction

CO₂ capture [1–3] is a very important issue at present. Liquid absorption has a high absorption capacity, but its high chemical activity leads to thermal degradation and equipment corrosion [4]. The use of solid adsorbents can avoid these disadvantages. Various types of solid adsorbents have been developed by many researchers to date. The main attention is paid to Li₂O [5], CaO [6, 7], which have a high chemical activity with respect to the carbon dioxide. However, these oxides have poor cyclic stability at high temperatures, resulting in reducing CO₂ adsorption capacity. Yoshikawa et al. [8, 9] showed that cerium dioxide adsorbed the largest CO₂ amount compared to other adsorbents based on silica and alumina. In a carbon dioxide atmosphere with water

vapor, bidentate carbonate and hydrocarbonate particles are mainly formed on the surface of the cerium dioxide, which have the lowest decomposition temperature, that makes it low energy consumption during the regeneration of the adsorbent. It is known that the adsorption properties are determined by the surface state of the metal oxide, which is characterized by the specific surface area, porosity, defectiveness, and texture. Textural characteristics depend on the preparation method of oxide adsorbent.

Cerium dioxide can be obtained from different precursors in three ways, i.e., gas-phase, solid-phase, and liquid-phase. For example, in gas-phase method, the synthesis occurs by evaporation of metallic cerium in vacuum with its further condensation in the cold zone and subsequent oxidation to cerium dioxide [10, 11]. In the solid phase method, CeO₂ can be obtained by thermolysis of cerium salts at high temperatures [12]. The decomposition of inorganic cerium compounds proceeds at higher temperatures compare to the organic cerium compounds. For example, the decomposition of Ce₂(CO₃)₃·8H₂O proceeds at temperature of 800–900 °C, while the decomposition of Ce(C₂H₅COO)₃·4H₂O proceeds at temperature of 270 °C. However, the use of organic cerium compounds leads to the contamination of cerium dioxide by the decomposition products of the organic residue. For example, cerium

✉ Yu-Wen Chen
ywchen@cc.ncu.edu.tw; ywchen@gmail.com

¹ National Research Tomsk State University, Tomsk 634050, Russian Federation

² National Research Tomsk Polytechnic University, Tomsk 634050, Russian Federation

³ Department of Chemical Engineering, National Central University, Zhongli 32001, Taiwan

dioxide obtained from cerium oxalate at 550 °C) is contaminated by Ce_4O_7 and carbon.

The decomposition of a colloidal solution of cerium hydroxide is widely used to produce cerium dioxide [13–16]. The colloidal suspension of cerium hydroxide [8, 17] is mainly obtained by precipitation with ammonia solution or alkali solution from cerium solutions. After decomposition and oxidation of cerium hydroxide to cerium dioxide, the cerium oxide is calcined at various temperatures for a long time in air. The use of ammonia solution as a precipitant has the advantage over alkali solutions, because it does not have impurities in cerium oxide due to the easy removal of the ammonium ion during heat treatment.

The use of microwave heating simplifies the technology of cerium dioxide obtaining from suspensions of cerium hydroxide [18–21]. Cerium dioxide is formed under mild temperature condition and less time. The microwave method makes it possible to obtain cerium dioxide and cerium dioxide doped with various elements with a high specific surface area, which is important for the adsorption properties of the material. In the structure of a highly dispersed CeO_2 sample obtained by decomposition of nitrate or hydroxide, the anionic sub-lattice is disordered due to the presence of NO_3^- and OH^- residual groups in it. These defects can stabilize the highly dispersed state of the oxide [22, 23]. High temperature heat treatment leads to the removal of defects, the sintering of particles and the decrease in the specific surface area.

The present study focused on the preparation of cerium dioxide and lanthanum-doped cerium dioxide adsorbents by microwave method for carbon dioxide adsorption. The influence of defect of CeO_2 and La-doped CeO_2 on the textural characteristics of the materials and their adsorption properties were investigated. The choice of lanthanum as the modified component was because that the chemical properties of lanthanum oxide are close to those of CaO , which exhibits a high chemical affinity for carbon dioxide. Therefore, the addition of lanthanum to the structure of cerium dioxide can increase the adsorption properties of the material. The change in the adsorption properties of cerium oxide modified with lanthanum was due to the formation of new defects. The lanthanum and cerium ions have almost the same atomic radius ($r(La^{3+}) = 0.104$ nm, $r(Ce^{3+}) = 0.102$ nm, $r(Ce^{4+}) = 0.088$ nm), that allows lanthanum to be incorporated into the cerium oxide crystalline structure to form new defects in the cationic sub-lattice.

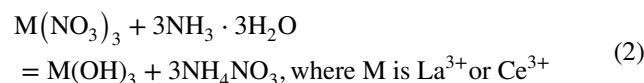
Experimental

Materials

Cerium nitrate hexahydrate (purity 99.9 wt%) and lanthanum nitrate hexahydrate (purity 99.9 wt%) were purchased from Novosibirsk plant of rare metals. Ammonia solution (24 wt%, chemically pure), hydrochloric acid solution (36 wt%, chemically pure), sodium carbonate (purity 99.9 wt%) and sodium hydroxide (purity 99.9 wt%) were purchased from ZAO Baza N°1. All reagents were used without further purification. Distilled water was used throughout the experiments.

Materials Preparation

Cerium dioxide and cerium dioxide doped with lanthanum ($CeO_2:La$) were prepared by exposure to microwave radiation on the suspensions of cerium hydroxide and lanthanum hydroxide. These hydroxides were obtained by precipitation with sodium hydroxide or an ammonia solution from aqueous solutions of Ce and La nitrates according to the following reactions:



The $Ce(NO_3)_3 \cdot 6H_2O$ and $La(NO_3)_3 \cdot 6H_2O$ salt were dissolved in 25 ml of distilled water each time with various La/Ce atomic ratios from 1.30 to 10.68 at.%. The concentrations of solutions were 0.7 mol/liter. Before the co-precipitation of $Ce(OH)_3$ and $La(OH)_3$, solutions of cerium nitrate with lanthanum nitrate were stirred for 2 h on a magnetic stirrer at room temperature. After stirring, sodium hydroxide solution or ammonia solution (2.1 mol/l) was added. The co-precipitation reaction produced a suspension with a purple solid. As can be seen from the equations, the resulting suspensions, in addition to metal hydroxides, contain sodium and ammonium nitrates, respectively. The suspension was placed in a microwave setup (frequency of 2.45 GHz and radiation power of 539 W) for 15 min. A yellow precipitate was obtained. The precipitate was filtered, washed with distilled water to remove the impurities and dried in the air at room temperature. The prepared samples were denoted as $CeO_2:La$ 1.30 at.%(NaOH), $CeO_2:La$ 3.16 at.%(NaOH), $CeO_2:La$ 9.50 at.%(NaOH), $CeO_2:La$ 1.30at.%(NH₃), $CeO_2:La$ 3.16 at.%(NH₃) and $CeO_2:La$ 9.50 at.%(NH₃) according to compositions and what precipitant were used. For comparison, the samples were prepared from pure $Ce(NO_3)_3$ and $La(NO_3)_3$ solutions and denoted as CeO_2

(NH₃), CeO₂ (NaOH), La(OH)₃ (NaOH) and La(OH)₃ (NH₃), respectively.

Materials Characterization

The phase composition and structure of the prepared samples were studied by X-ray diffraction (XRD) using a Rigaku Miniflex 600 (Japan) with a CuK α source ($\lambda = 1.5418 \text{ \AA}$) and monochromator. The diffraction pattern was scanned by steps of 0.02° , recording rate of 2° min^{-1} in the 2θ range from 10 to 90° . The qualitative phase composition was determined using the PCPDFWIN database and the full-profile analysis program POWDER CELL 2.4. The structure was refined by the Rietveld method, precision method and least squares method using the ReX Powder diffraction program. The crystallite size was calculated using the POWDER CELL 2.4 program and the Scherrer's equation:

$$D_{XRD} = K_\lambda / \beta \cos \theta \quad (3)$$

where D_{XRD} is the crystallite size; K is a dimensionless shape factor with a value close to unity; λ is the X-ray wavelength; β is line broadening at half maximum intensity. The type of solid solution CeO₂:La was determined based on the XRD results (interplanar spacing, crystal lattice parameter) using Vegard's law. The type of solid solution was determined by calculating the number of atoms of the unit cell using the formula:

$$n = \frac{V_c \rho}{A_{av.} \cdot 1.66 \cdot 10^{-24}} \quad (4)$$

where V_c is the unit cell volume, $A_{av.}$ is the weighted average atomic mass, ρ is the density of the substance, $1.66 \cdot 10^{-24}$ is 1/16 of the mass of an oxygen atom. Based on the obtained value of n , the type of solid solution was determined: $n = 1, 2, 4 \dots$, i.e., an integer rational number and coincides with the theoretical value for a given lattice (the cell volume may differ from the theoretical one). This situation is typical for a substitutional solid solution. If n is more than $n_{\text{theor.}}$, the solid solution is an interstitial solid solution. The formation of interstitial solid solutions is always accompanied by an increase in the unit cell volume. For a subtraction solid solution the value $n < n_{\text{theor.}}$ and it is unstable. The pycnometric method was used to determine the density of the obtained samples. Density was calculated using the formula:

$$\rho = \frac{m}{M_0 - M + m} \rho_0 \quad (5)$$

where m is the mass of the test sample, M_0 and ρ_0 are the mass and density of the solvent, respectively, M is the mass of the pycnometer filled with the solvent. Toluene was used as a solvent.

The surface morphology of samples was studied by scanning electron microscopy (SEM). The distribution of elements on the surface was determined by energy dispersive X-ray spectroscopic (EDS) analysis. These analyses were performed using Hitachi TM-3000 scanning electron microscope with attachment Quantax 70 for X-ray microanalysis (Hitachi High-Technologies Corporation, Japan). The particle sizes of cerium dioxide and cerium dioxide doped with lanthanum and the time of their settling from suspension were determined by the method of sedimentation analysis. Sedimentation analysis was carried out using the Scanning photosedimentograph SF-2 M. The particle size was calculated using the formula:

$$r = \sqrt{\frac{9\eta u}{2(D-d)g}} \quad (6)$$

where r is the equivalent particle radius; η is the viscosity of the medium; u is the linear velocity of the particle; D and d are the densities of the dispersed phase and the dispersed medium; g is the acceleration due to gravity.

The specific surface area, porosity and other textural characteristics of the samples were studied by low-temperature adsorption-desorption N₂ method on a TriStar II Micromeritics device. The specific surface area was determined by the Brunauer-Emmett-Teller (BET) multi-point method in the range of P/P^0 from 0.05 to 0.30. Pore size distribution plots were plotted using the Barrett-Joyner-Halund (BJH) method with the adsorption branch isotherm analysis. Before measurements, the sample (200 mg) was degassed in vacuum at 200°C for 2 h. The IR and Raman spectra of the samples were obtained with Nicolet 6700 spectrophotometer (USA) in the range from 400 to 4000 cm^{-1} to study the formation of the bonds in the composites. The acid-base properties of the surface of CeO₂ and La-modified CeO₂ were determined using a Multitest pH meter with a combined ESC-10605 glass electrode (made in Russia). Synchronous thermal analysis of samples was conducted using an STA 449 F1 Jupiter thermoanalyzer interfaced with a QMS 403 Aolos gas mass spectrometer (Netzsch-Gertebau GmbH, Germany) and allowed to establish thermal stability and the absence (presence) of impurities in the samples. The samples were heated from 25 to 1000°C in air at a heating rate of $10^\circ \text{C min}^{-1}$. The measurements for each sample were conducted at least twice.

Carbon dioxide was produced in the equipment that is shown in Fig. 1. The investigated solid material ($m = 0.2 \text{ g}$) was added into the flasks. The flasks were filled with the resulting carbon dioxide, and kept for 20 min. After that, the IR spectra of the samples were obtained.

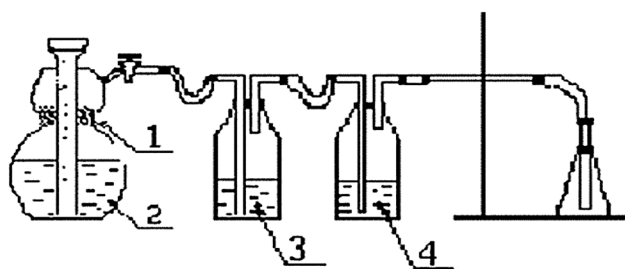


Fig. 1 The equipment for the production of carbon dioxide. (Kipp apparatus: 1— Na_2CO_3 powder, 2—hydrochloric acid solution, 3—Tishchenko flask with H_2SO_4 conc. solution, 4—Tishchenko flask with NaOH conc. solution)

A quantitative assessment of the carbon dioxide sorption capacity of the samples was carried out by changing the volume of CO_2 in a reaction vessel containing $\text{CeO}_2\text{:La}$ (1.3 at.%) and $\text{CeO}_2\text{:La}$ (9.5 at.%) powders. Samples of cerium dioxide or solid solutions of the same mass were placed in the autoclave (volume 50 ml) with a pressure sensor. The autoclave was then filled with carbon dioxide. The carbon dioxide was monitored by changing the pressure in the autoclave. Sorption was carried out for 2 h at room temperature and atmospheric pressure of 100.39 kPa. The volume of carbon dioxide was recalculated to normal conditions of 273 K, 101,31 kPa and 1 g of sorbent.

Results and Discussion

Composition and Structure of CeO_2 and La-CeO_2 Samples

X-ray diffraction patterns of the samples are shown in Fig. 2. The diffraction peaks (Fig. 2a, b) of samples obtained under microwave action on the suspensions $\text{Ce}(\text{OH})_3$ with NaNO_3 or NH_4NO_3 , correspond to cubic cerium dioxide. The results of XRD phase analysis (Fig. 2c) indicate that microwave treatment of suspensions of $\text{La}(\text{OH})_3$ with NaNO_3 or NH_4NO_3 , under the same conditions, did not lead to the formation of La_2O_3 . On the diffraction pattern (Fig. 2c), the maxima correspond to the lanthanum hydroxide phase of the pyrochlore structure. Lanthanum oxide was not formed from lanthanum hydroxide, probably due to insufficient thermal energy generated when the suspension interacts with microwave radiation. As can be seen from Table 1, the decomposition reaction of cerium hydroxide is under normal conditions but the changes in the Gibbs free energy and enthalpy of the decomposition reaction of lanthanum hydroxide are quite high, and under normal conditions, the thermal destruction is impossible.

According to the literature data [24], the decomposition temperature of lanthanum hydroxide in the solid state is

from 300 to 1100 °C. All this suggests that the temperature of the suspension of lanthanum hydroxide with sodium nitrate or ammonium nitrate during the microwaves heating at radiation power of 539 W and frequency of 2.45 Hz for 15 min does not reach the decomposition temperature of the $\text{La}(\text{OH})_3$. It was not possible to prepare $\text{CeO}_2\text{:La}$ solid solutions from the suspension of $\text{Ce}(\text{OH})_3$ with $\text{La}(\text{OH})_3$ and NH_4NO_3 . According to the XRD results, the mixture of cerium dioxide with lanthanum hydroxide formed at this synthesis conditions (Fig. 2d). Using the sodium hydroxide as a precipitant under the presented conditions of microwave exposure made it possible to prepare $\text{CeO}_2\text{:La}$ solid solutions (Fig. 2e–g) with a lanthanum content less than 9.50 at.%. Besides the peaks assigned to CeO_2 in the diffraction pattern of $\text{CeO}_2\text{:La}$ 10.68 at.%(NaOH) sample, there is a characteristic XRD peak of the lanthanum hydroxide phase, so this sample is a mixture of substances.

When the diffraction patterns of all $\text{CeO}_2\text{:La}(\text{NaOH})$ samples are superimposed, a shift of the diffraction peaks towards larger angles was observed with an increase in the lanthanum content from 1.30 to 9.50 at.% (Fig. 3), indicating the incorporation of lanthanum into the crystalline structure of CeO_2 . In addition, there was a change in the values of the lattice parameter: the values increased with the increase of lanthanum content (Table 2).

To calculate the number of atoms per unit cell, the density of $\text{CeO}_2\text{:La}$ solid solutions was determined by the pycnometric method (Table 3). As the lanthanum content in the solid solution increase, the density of the samples decreases from 7.00 to 6.66 g/cm^3 . The number of atoms per unit cell does not change, indicating the formation of a substitutional solid solution. Figure 4 shows the dependences of the crystal cell parameters of $\text{CeO}_2\text{:La}$ samples on the lanthanum content. The resulting dependences are linear, which corresponds to Vegard's rule for substitutional solid solutions.

Using the Vesta program, it was established that CeO_2 and $\text{CeO}_2\text{:La}$ samples have the same structural characteristics: the number of atoms is 270, the number of connections is 832 and the number of polyhedra is 14. The crystalline structures of the samples were built according to the refined parameters (Fig. 5).

According to the results, it shows that the value of the structural characteristics of the unit cell of cerium dioxide did not change when the lanthanum ion was incorporated into the crystalline structure of cerium oxide. It confirms the previously determined type of substitutional solid solution. The number of oxygen atoms in the solid solutions was determined using Kim's empirical equation [25, 26]:

Fig. 2 X-ray diffraction patterns of the samples: **a** CeO₂ (NaOH), **b** CeO₂ (NH₃), **c** La(OH)₃, **d** CeO₂:La 1.30 at. % (NH₃), **e** CeO₂:La 1.30 at. % (NaOH), **f** CeO₂:La 3.16 at. % (NaOH), **g** CeO₂:La 9.50 at. % (NaOH)

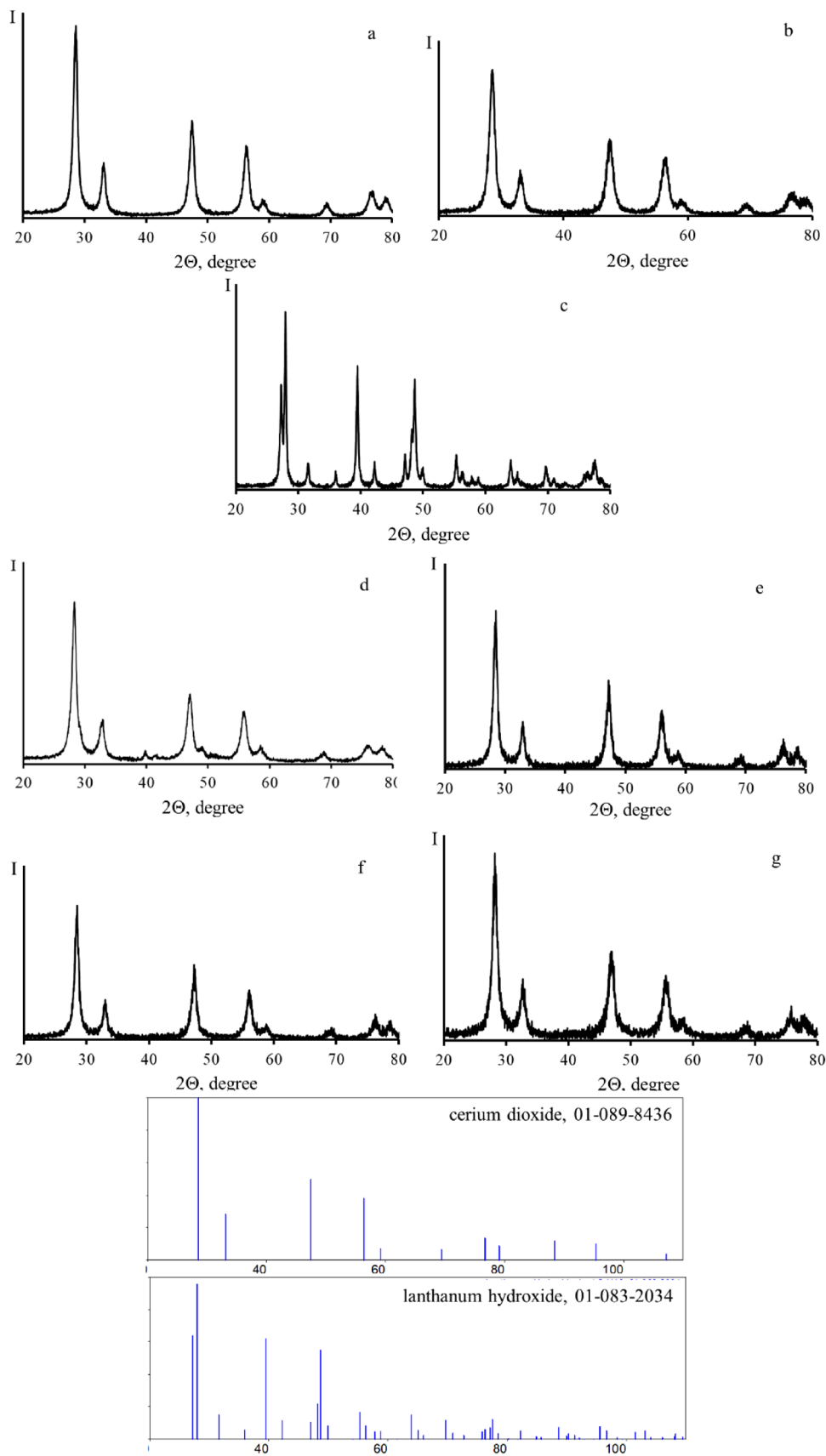


Table 1 The values of thermodynamic functions for decomposition reactions of La(OH)₃ and Ce(OH)₃

Reaction	ΔH _f (kJ/mol)	S _f (J/mol K)	ΔG _f (kJ/mol)
2La(OH) _{3(sol.)} = La ₂ O _{3(trb.)} + 3H ₂ O _(g.)	199.27	-399.2	1067.37
4Ce(OH) _{3(sol.)} + O _{2(g.)} = 4CeO _{2(sol.)} + 6H ₂ O _(g.)	-594.66	-80.51	-366.62

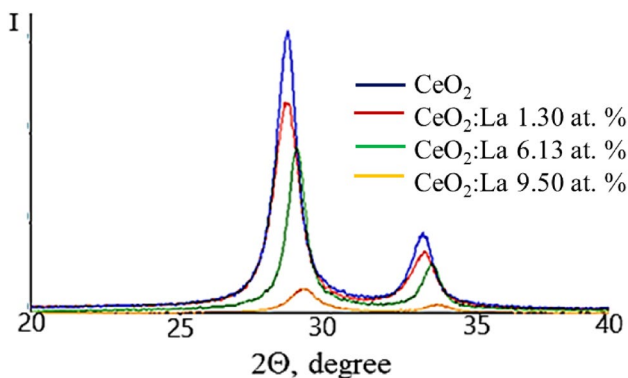


Fig. 3 Diffractograms of the samples

Table 2 Crystallographic parameters of CeO₂ and CeO₂:La solid solution

La content, at. %	Lattice diameter a, Å		
	Precision method	Rietveld method	Least square method
0	5.4031	5.4097	5.3984
1.30	5.4187	5.4122	5.4140
3.16	5.4277	5.4205	5.4224
9.50	5.4901	5.4837	5.4853

Table 3 Sample density (ρ) and number of atoms per unit cell (n)

La content, at. %	ρ ± 0.02, g/cm ³	n ± 0.2
0	7.00	11.6
1.30	6.87	11.5
3.16	6.72	11.5
9.50	6.66	11.6

$$a(nm) = 0.5413 + 0.04612x \tag{7}$$

where *a* is the lattice parameter, *x* is the number of [O] atoms. So, the solid solution corresponds to the formula

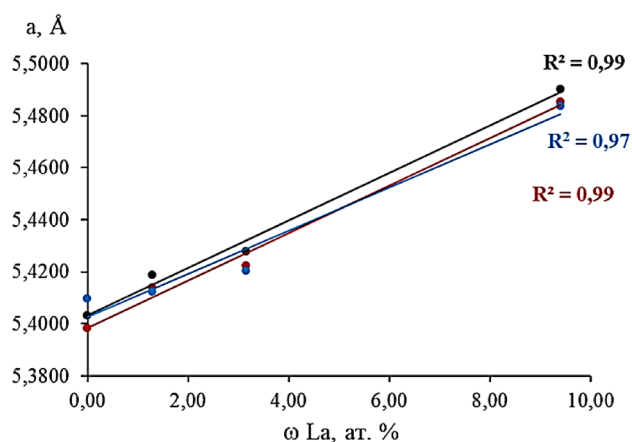


Fig. 4 Dependences of the cell parameter on the lanthanum content: 1—the experimental data (black curve); 2—the corrected data by the Rietveld method (blue curve); 3—the updated data of the least squares (red curve)

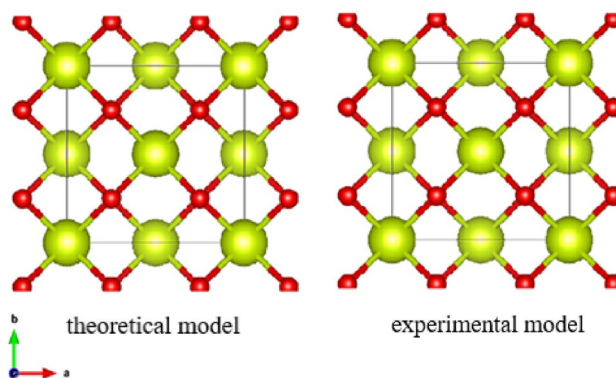


Fig. 5 Crystallographic structure of CeO₂ and CeO₂:La

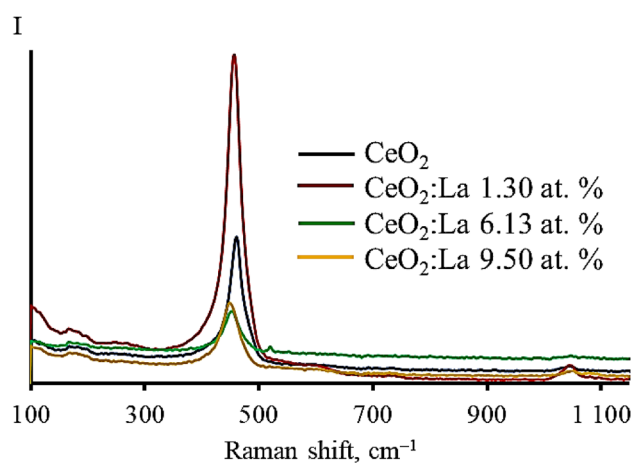


Fig. 6 Raman spectra of the samples

Ce_{1-x}La_xO_{1.96}-Ce_{1-x}La_xO_{1.83} with a lanthanum content of between 1.30 and 9.50 at.%.

Figure 6 shows Raman spectra of the undoped and the La-doped CeO₂ samples. The ~465 cm⁻¹ peak was attributed to the F_{2g} vibrational mode of Ce-O8 light, a key internal phonon mode for the Fm3m fluorite structure [27].

The spectra show an increase in the full width at half maximum (FWHM) of this Raman peak in La-doped CeO₂ samples compared to the undoped one. The change in the FWHM indicates that the defectiveness of the samples structure is different. With an increase in the content of lanthanum, the number of oxygen vacancies in the structure of the solid solution increases. In addition, the spectra exhibited shifts of the F_{2g} peak upon doping La, the main reason for which is the difference in ionic radius of the doped element. Moreover, as the crystallite size decreases, the weight of off-center phonons increases, and the phonon distribution causes an asymmetric expansion and shift of the Raman scattering mode [28, 29]. These results are consistent with the results of XRD analysis.

According to the SEM and EDS results, the uniform distributions of lanthanum together with cerium and oxygen were observed over the surface of all the samples (Fig. 7 and Table 4).

The results of EDS analysis and the calculated amount of oxygen in solid solutions with different lanthanum contents are opposite. The overestimated oxygen content is probably due to the presence of oxygen-containing impurities in the fluorite structure, the content of which increased with an increase in the lanthanum content.

The mass spectra of the gaseous decomposition products also confirmed the presence of impurities in the composition of such samples. The TGA and DSC curves, and the mass spectra of the products of thermal decomposition of CeO₂ and CeO₂:La 9.5 at.% samples are shown in Fig. 8.

The decrease in mass was observed on the TGA curves of these samples in the temperature range of 25–800 °C. Thermal destruction of samples proceeds in three stages. The weight loss of the CeO₂ sample is 2.65 wt%, and the weight loss of the CeO₂:La 9.50 at.% sample is 3.04 wt%. According to the mass spectra, the gaseous decomposition products of the samples are characterized by $m/z = 44$ and $m/z = 18$ corresponding to water and carbon dioxide, which are removed with an endothermic reaction with a maximum at $T = 71\text{--}74$ °C. Such a low-temperature value evidences that on the surface of the samples, there are water and carbon dioxide molecules physically adsorbed from air. The m/z values of 46 and 30 and the identical mass spectra indicate that nitrogen dioxide exists in the gas phase [30]. The removal of nitrogen dioxide from the structure of CeO₂ and CeO₂:La occurs in two stages with endothermic reaction. If the presence of water and carbon dioxide on the surface of cerium dioxide or solid solution

of cerium dioxide with lanthanum can be explained by their sorption from air, the presence of nitrogen dioxide is due to the presence of impurities of nitrate groups in the anionic sublattice [22].

Surface and Textural Characteristics of CeO₂ and CeO₂:La Samples

The average particle size of the samples decreased from 4.4 μm to less than 1 μm with an increase of lanthanum content in the solid solution from 0 to 9.50 at.% (Table 5). The values of coherent scattering regions (CSR) values calculated by the Scherrer's equation from XRD results (Table 5) demonstrate the same regularity.

The results of the sedimentation analysis of CeO₂ and CeO₂:La samples with different contents of lanthanum are shown in Fig. 9.

The analysis of the particle size distributions of the samples shows that the number of particles smaller than 1 μm increased with increasing lanthanum content. Cerium dioxide, for example, contains 30% of particles with a size of less than 1 μm; and the CeO₂:La (3.16 at.%) sample has 60% (Fig. 9). The content of the largest particles decreases accordingly. The prepared samples are characterized by a relatively low specific surface area, which increases with increasing lanthanum content in the solid solution (Table 6).

As can be seen from the data presented in Table 6, the pore size and pore volume increased with the addition of lanthanum. Figure 10 shows isotherms of nitrogen sorption on the surface of the samples. The resulting type of isotherms belongs to type V according to the classification of Brunauer, Deming, and Taylor [31–33]. The type of hysteresis loops is characteristic of cylindrical pores with a weak adsorbent–adsorbate interaction.

The results of IR spectroscopy (Fig. 11) confirm the assumptions about the presence of adsorbed water and carbon dioxide molecules on the surface of cerium dioxide and the solid solution of cerium dioxide modified with lanthanum.

The absorption bands at 3550–2455 and 1600 cm⁻¹ indicate stretching and bending vibrations of the bonds of the OH-groups of water molecules (Fig. 11). The absorption bands in the 1500–800 cm⁻¹ region can be attributed to the bonds vibrations of CO₃²⁻ group [8, 34]. The analysis of all peaks (818 cm⁻¹, 1026 cm⁻¹, 1340 cm⁻¹, and 1467 cm⁻¹) in this region for CeO₂ samples suggests that two carbonate forms are mainly present on the oxide surface, i.e., bidentate carbonate and polydentate carbonate. The addition of lanthanum to cerium dioxide did not lead to the change of carbonate forms on the surface of the samples. Only a slight shift of the absorption band maxima was observed on the IR spectra of these samples, compared with the IR spectrum

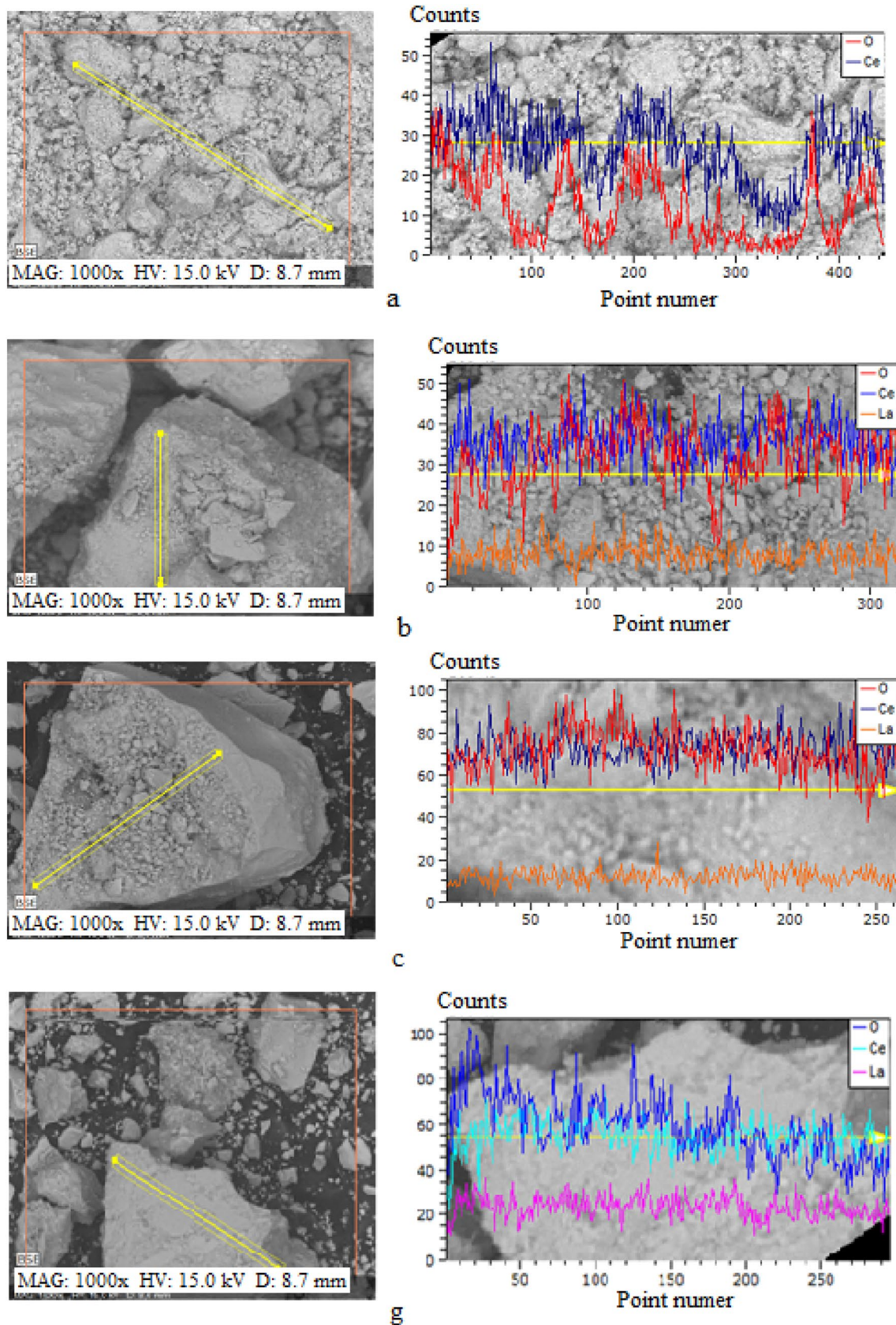


Fig. 7 Linear profile of the element distributions on the surface of the samples: a – CeO_2 , b – $\text{CeO}_2\text{:La}$ 1.30 at. %, c – $\text{CeO}_2\text{:La}$ 3.16 at. %, g – $\text{CeO}_2\text{:La}$ 9.50 at. %

Table 4 Results of quantitative analysis

Sample/ element	CeO ₂ 0 at.% La	CeO ₂ :La 1.30 at.% La	CeO ₂ :La 3.16 at.%	CeO ₂ :La 9.50 at.%
	content, at.%			
Ce	40.92	26.52	22.16	15.25
O	59.08	72.24	74.78	75.59
La	—	1.24	3.06	9.16

of CeO₂. However, the intensity of the water absorption bands increased, which is explained by the large amount of adsorbed water from the air adsorbed on the surface of CeO₂:La samples.

Adsorption Properties of CO₂ on CeO₂ and CeO₂:La Samples

To study the sorption properties, the samples were annealed at 300 and 600 °C before experiment. These temperatures were chosen based on the results of thermal analyzes with mass spectrometry. The study showed that the carbonate ion was completely removed from the surface of the samples up to 300 °C. The impurities of the nitro group in the anionic sub-lattice of cerium oxide and the solid solution were completely removed from their structure at 600 °C.

The samples annealed at 300 °C for 2 h were immediately placed in a carbon dioxide atmosphere for 90 min. The IR spectra of the samples were taken every 30 min. The results of IR spectra are shown in Fig. 12. The significant change in the IR spectra for all the samples was

Fig. 8 TGA and DSC curves and mass spectra of samples: **a** CeO₂; **b** CeO₂:La 9.5 at.%

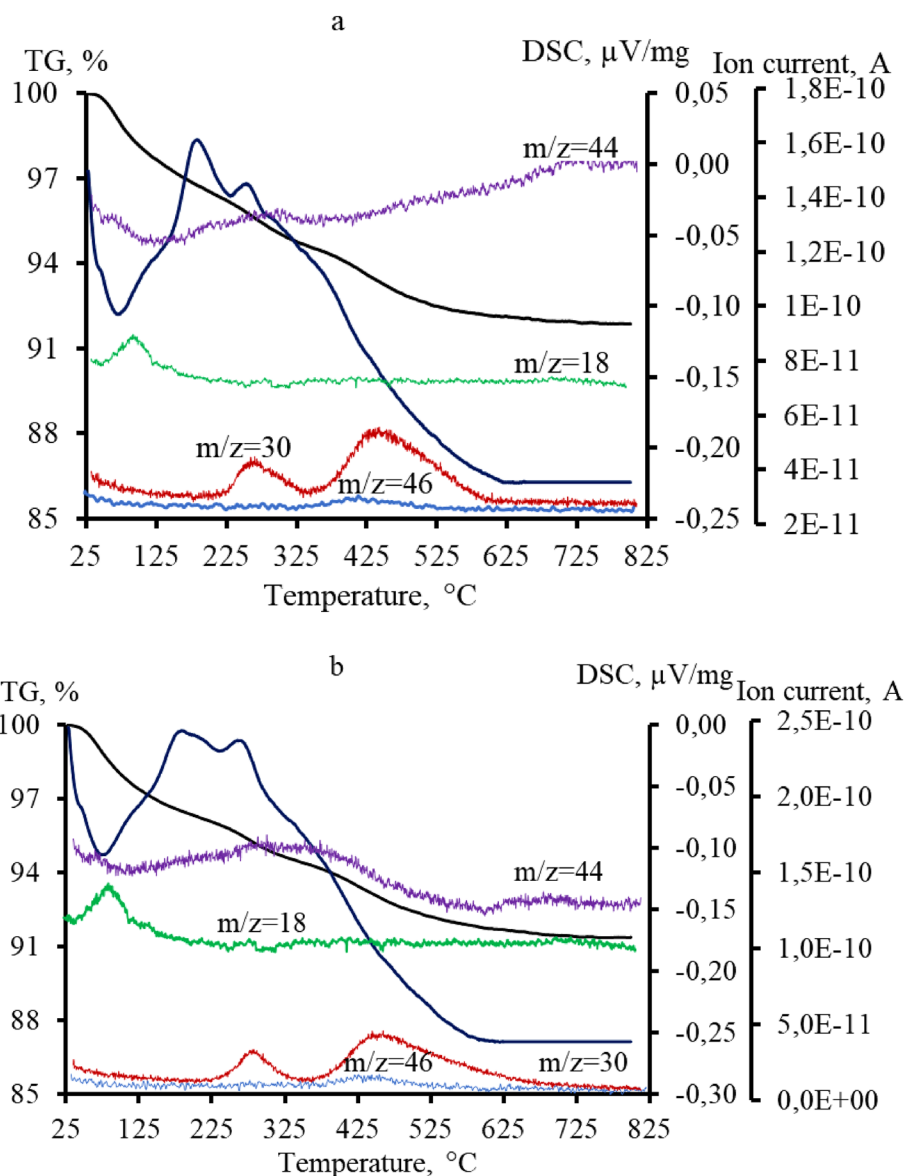


Table 5 Particle sizes and CSR values of the CeO₂ и CeO₂:La samples

	CeO ₂	CeO ₂ :La 1.30 at. %	CeO ₂ :La 3.16 at. %	CeO ₂ :La 9.50 at. %
Average particle size, μm (by sedimentation method)	4,467	2,773	1,235	< 1
CSR, nm (by XRD method)	8,3	7,3	6,6	6.8

observed only within 60 min. During this time, the surface was completely saturated with carbonate ions. The analysis of the maximum absorption coefficients of carbonate ions from the IR spectra of the samples indicates that the sorption properties of the cerium dioxide and cerium dioxide doped with lanthanum samples are similar. The forms of carbonate ions during sorption did not change with time. However, a shift in the adsorption frequencies corresponding to carbonate ion to the high-frequency region was observed. This fact indicates that the amount of adsorbed bidentate carbon dioxide increased with increasing lanthanum content in the La-CeO₂ samples. Preliminary analysis showed that CO₂ adsorption on the studied samples is reversible at a temperature of 300 °C.

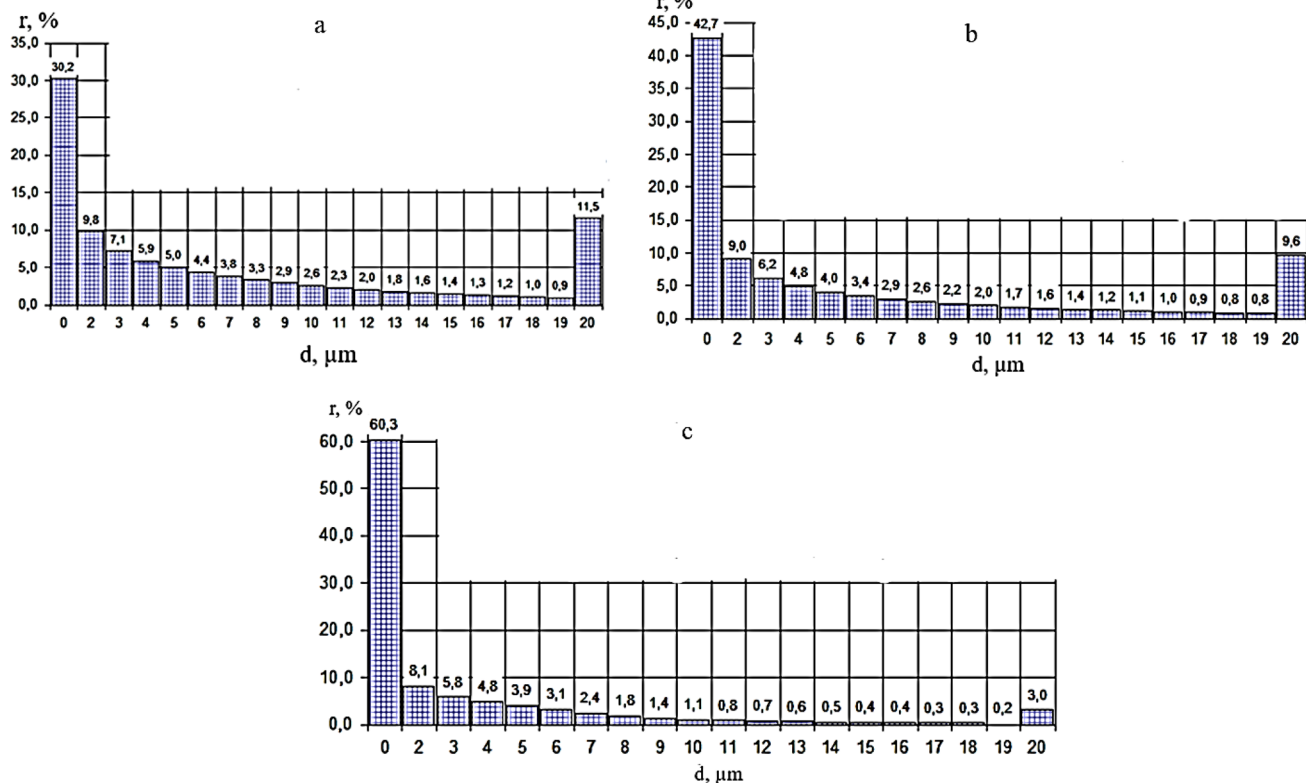
Annealing the samples at 600 °C for 2 h reduced the number of oxygen vacancies in the solid solutions and their specific surface area to 5–7 m²/g. The samples annealed at 600 °C did not exhibit high adsorption properties with respect to carbon dioxide, since the surface area was too low.

Figure 13 shows curves of changes in CO₂ content over time as a result of sorption by CeO₂:La (1.30 at. %) and CeO₂:La (9.50 at. %) samples annealed at 300 °C.

The reproducibility of the sorption results was 3.3% of the equilibrium values for each sample. For the same sample, 5 cycles and measurements were performed). Rapid CO₂ absorption is observed during the first 30–50 min.

Table 6 Results of analysis of nitrogen sorption by the BET method

Sample	La content, at. %	S _{yt} , m ² /g Δ ± 10%	Total pore volume, cm ³ /g	Average pore size, nm
CeO ₂	0	21.4	0.070	41.7
CeO ₂ :La	1.30	25.3	0.140	22.0
CeO ₂ :La	3.16	39.5	0.195	30.0
CeO ₂ :La	9.50	53.2	0.359	39.7

**Fig. 9** Particle size distribution of samples: **a** CeO₂, **b** CeO₂:La 1.30 at. %, **c** CeO₂:La 3.16 at. %

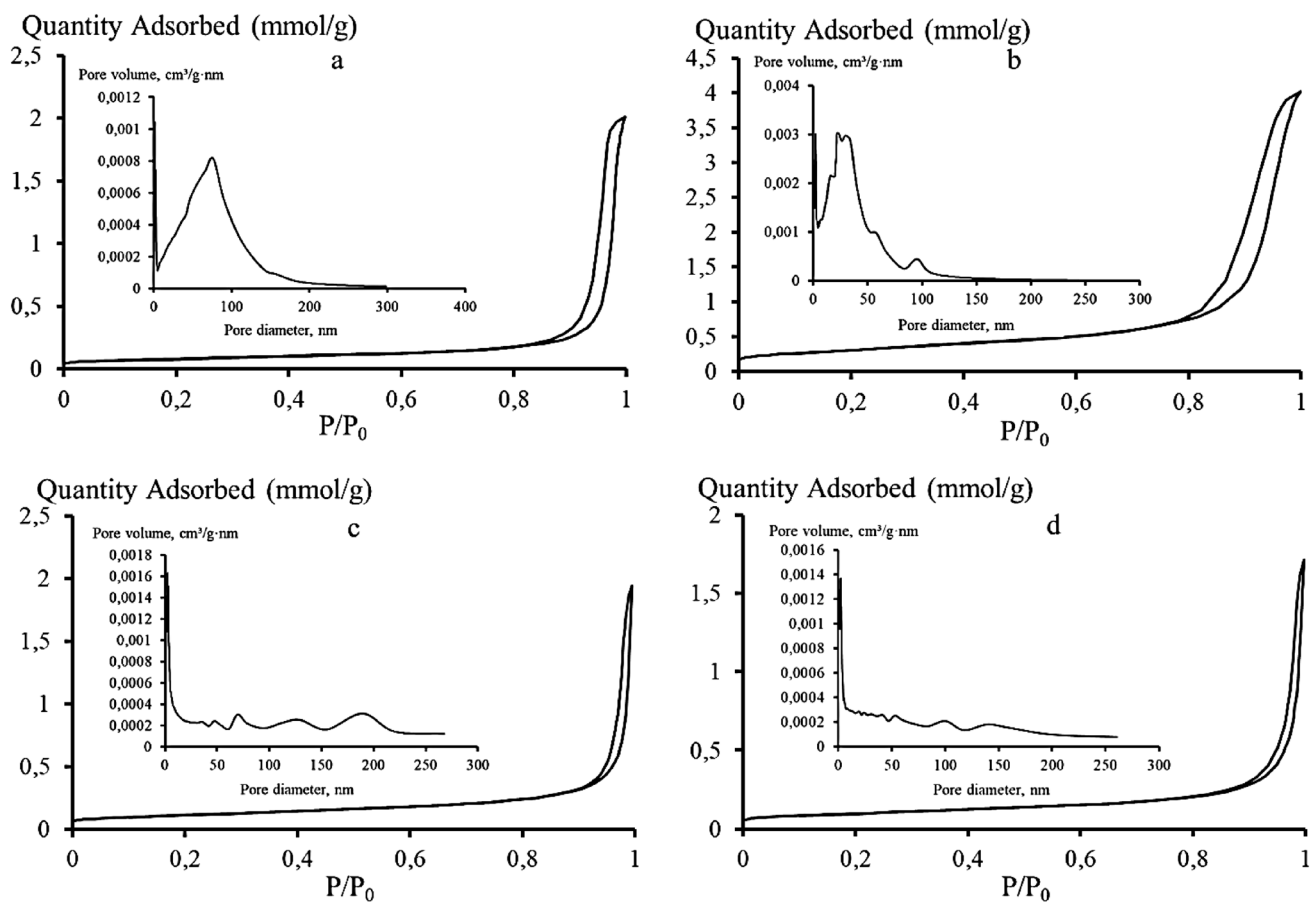


Fig. 10 Adsorption–desorption isotherms of samples: **a** CeO₂, **b** CeO₂:La 1.30 at. %, **c** CeO₂:La 3.16 at. %, **d** CeO₂:La 9.50 at. %

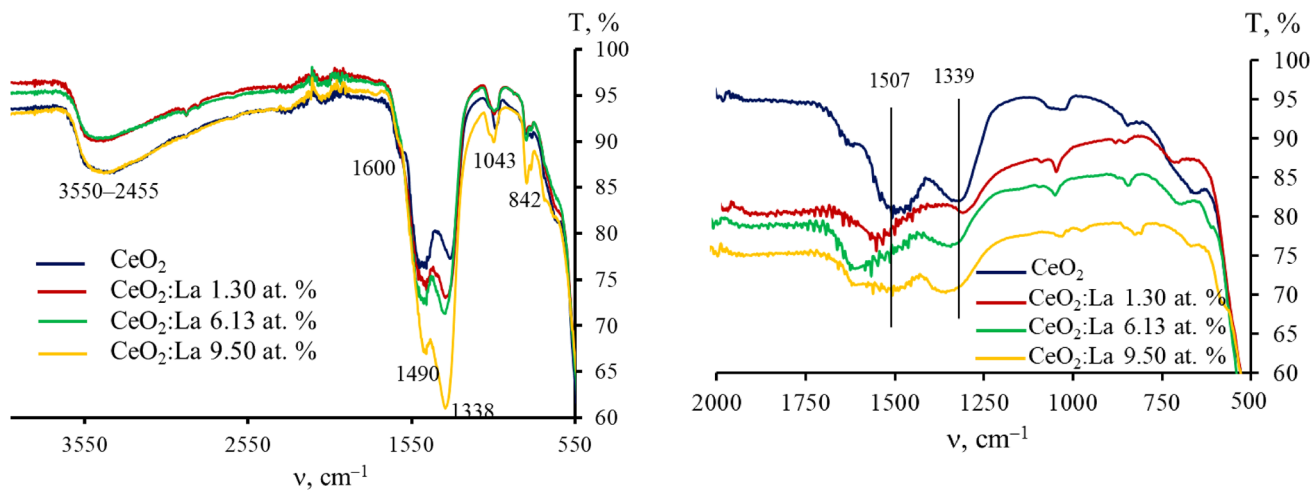


Fig. 11 IR transmission spectra of the samples

Fig. 12 IR transmission spectra of samples aged for 60 min in a CO₂ atmosphere

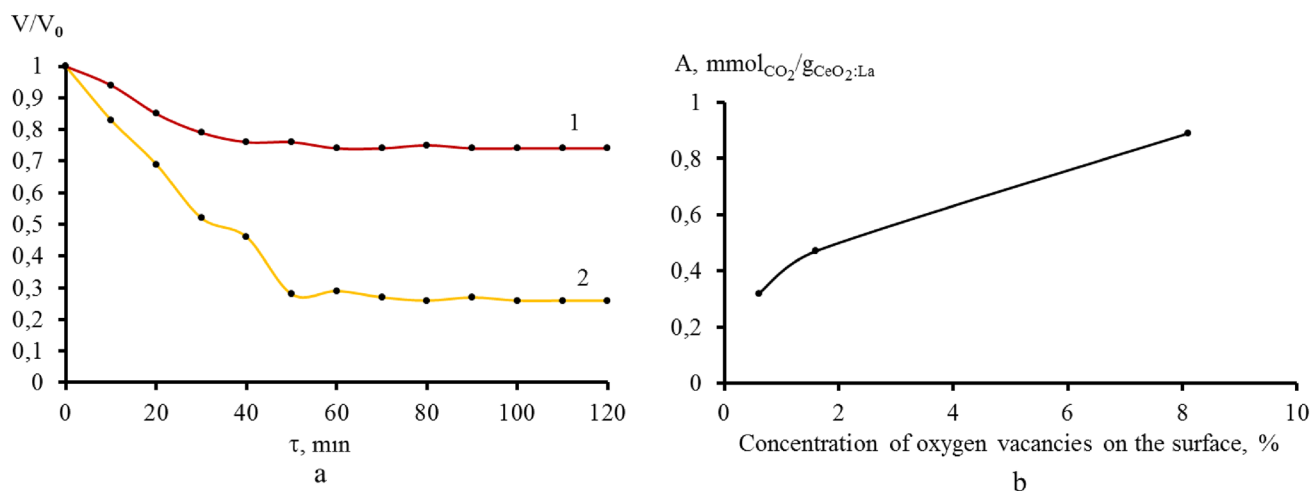


Fig. 13 Variation of the CO₂ content absorbed by the samples as a function of their exposure time (a): 1—CeO₂:La (1.30 at.%), 2— CeO₂:La (9.50 at.%) and relationship between CO₂ adsorption and surface oxygen vacancy concentration (b)

This is followed by a slower sorption process, which ends at 60–65 min. The obtained regularities of the influence of the number of oxygen vacancies on the sorption capacity of the surface of the solid solution based on cerium dioxide with lanthanum (Fig. 13b), are in agreement with the results of the researchers Bin Liu et al. [35] on the sorption of CO₂ on the surface of the solid solution of cerium dioxide with zirconium addition. The increase in oxygen vacancies leads to an increase in the CO₂ sorption coefficient. This further demonstrates the significance of the presence of oxygen vacancies in the oxide structure for CO₂ sorption.

Conclusion

This study showed the preparation method of CeO₂:La (1.30–9.50 at.%) solid solutions from aqueous suspensions of cerium (III) and lanthanum hydroxides by microwave method (radiation power 539 W, frequency 2.45 Hz). These hydroxides were prepared by precipitation with sodium hydroxide from Ce(NO₃)₃ and La(NO₃)₃ solution. After 15 min of microwave exposure to suspensions, the cerium and lanthanum hydroxides decomposed and formed cubic crystalline structures of CeO₂ and CeO₂:La (1.30–9.50 at.%) solid solutions. Increasing the lanthanum content of the solid material leads to a reduction in particle size and an increase in the specific surface area of the samples. The samples contain nitrate ions in their structure as the impurity.

All samples adsorbed carbon dioxide molecules on the surface as bidentate and poly dentate forms, which were stable up to 300 °C. The samples retain their adsorption properties after thermal treatment at 300 °C. The increase

in the content of lanthanum in the CeO₂:La solid solution leads to the increase in the number of oxygen vacancies in the crystalline structure and the increase in the adsorption capacities of carbon dioxide in the form of bidentate forms compared to the undoped CeO₂. The samples annealed at 600 °C reduces oxygen vacancies and lowers surface area, resulting in the absence of adsorption capacities of the samples to carbon dioxide.

Author Contributions SAK—author responsible for setting the goal and description of the results, OSK—author responsible for the analysis and description of the results, AGM—author responsible for the analysis and description of the results, Y-WC—editing and revising the manuscript.

Funding This study was supported by the Tomsk State University Development Programme (Priority-2030).

Data Availability The authors will provide data and materials upon request.

Declarations

Conflict of Interests The authors declare that they have no known competing financial interests or personal relationships that could have appeared to influence the work reported in this paper.

Ethical Approval Not Applicable.

References

1. F.O. Ochedi, Y. Liu, Y.G. Adewuyi, State-of-the-art review on capture of CO₂ using adsorbents prepared from waste materials. *Proc. Saf. Environ. Protect.* **139**, 1–25 (2020). <https://doi.org/10.1016/j.psep.2020.03.036>

- R. Ahmed, G. Liu, B. Yousaf, Q. Abbas, H. Ullah, M.U. Ali, Recent advances in carbon-based renewable adsorbent for selective carbon dioxide capture and separation—a review. *J. Clean. Prod.* **242**, 118409 (2020). <https://doi.org/10.1016/j.jclepro.2019.118409>
- S.G. Subraveti, S. Roussanaly, R. Anantharaman, L. Riboldi, A. Rajendran, How much can novel solid sorbents reduce the cost of post-combustion CO₂ capture? A techno-economic investigation on the cost limits of pressure–vacuum swing adsorption. *Appl. Energy* **306**, 117955 (2022). <https://doi.org/10.1016/j.apenergy.2021.117955>
- C.-H. Yu, C.-H. Huang, C.-S. Tan, A Review of CO₂ capture by absorption and adsorption, aerosol and air. *Qual. Res.* **12**, 745–769 (2012). <https://doi.org/10.4209/aaqr.2012.05.0132>
- Y. Hu, W. Liu, Z. Zhou, Y. Yang, Preparation of Li₄SiO₄ sorbents for carbon dioxide capture via a spray-drying technique. *Energy Fuels* **32**, 4521–4527 (2018). <https://doi.org/10.1021/acs.energyfuels.7b03051>
- J. Shi, Y. Li, Q. Zhang, X. Ma, L. Duan, X. Zhou, CO₂ capture performance of a novel synthetic CaO/sepiolite sorbent at calcium looping conditions. *Appl. Energy* **203**, 412–421 (2017). <https://doi.org/10.1016/j.apenergy.2017.06.050>
- K. Liu, B. Zhao, Y. Wu, F. Li, J. Zhang, Bubbling synthesis and high-temperature CO₂ adsorption performance of CaO-based adsorbents from carbide slag. *Fuel* **269**, 117481 (2020). <https://doi.org/10.1016/j.fuel.2020.117481>
- K. Yoshikawa, H. Sato, M. Kaneeda, J.N. Kondo, Synthesis and analysis of CO₂ adsorbents based on cerium oxide. *J. CO₂ Utilization* **8**, 34–38 (2014). <https://doi.org/10.1016/j.jcou.2014.10.001>
- Y. Shan, Y. Liu, Y. Li, W. Yang, A review on application of cerium-based oxides in gaseous pollutant purification. *Sep. Purif. Technol.* **250**, 117181 (2020). <https://doi.org/10.1016/j.seppur.2020.117181>
- A. Tschöpe, J.Y. Ying, Synthesis of nanostructured catalytic materials using a modified magnetron sputtering technique. *Nanostruct. Mater.* **4**, 617–623 (1994). [https://doi.org/10.1016/0965-9773\(94\)90071-X](https://doi.org/10.1016/0965-9773(94)90071-X)
- G. Adachi, N. Imanaka, The binary rare earth oxides. *Chem. Rev.* **98**, 1479–1514 (1998). <https://doi.org/10.1021/cr940055h>
- X. Yu, F. Li, X. Ye et al., Synthesis of cerium (IV) oxide ultrafine particles by solid-state reactions. *J. Am. Ceram. Soc.* **83**, 964–966 (2000). <https://doi.org/10.1111/j.1151-2916.2000.tb01306.x>
- F. Zhang, S.W. Chan, J.E. Spanier et al., Cerium oxide nanoparticles: size selective formation and structure analysis. *Appl. Phys. Lett.* **80**, 127–129 (2002). <https://doi.org/10.1063/1.1430502>
- P.L. Chen, I.W. Chen, Reactive cerium (IV) oxide powders by the homogeneous precipitation method. *J. Am. Ceram. Soc.* **76**, 1577–1583 (1993). <https://doi.org/10.1111/j.1151-2916.1993.tb03942.x>
- T.C. Rojas, M. Ocana, Uniform nanoparticles of Pr (III)/Ceria solid solutions prepared by homogeneous precipitation. *Scripta Mater.* **46**, 655–660 (2002). [https://doi.org/10.1016/S1359-6462\(02\)00047-7](https://doi.org/10.1016/S1359-6462(02)00047-7)
- H. Li, G. Wang, F. Zhang, Y. Cai, Y. Wang, I. Djerdj, Surfactant-assisted synthesis of CeO₂ nanoparticles and their application in wastewater treatment. *R. Soc. Chem.* **2**, 12413–12423 (2012). <https://doi.org/10.1039/c2ra21590j>
- L.S.R. Rocha, R.A.C. Amoresi, T.M. Duarte, N.L. Marana, J.R. Sambrano, C.M. Aldao, A.Z. Simões, M.A. Ponce, E. Longo, Experimental and theoretical interpretation of the order/disorder clusters in CeO₂:La. *Appl. Surf. Sci.* **510**, 145216 (2020). <https://doi.org/10.1016/j.apsusc.2019.145216>
- S. Mishra, S. Soren, A.K. Debnath, D.K. Aswal, N. Das, P. Parhi, Rapid microwave—hydrothermal synthesis of CeO₂ nanoparticles for simultaneous adsorption/photodegradation of organic dyes under visible light. *Optik* **169**, 125–136 (2018). <https://doi.org/10.1016/j.ijleo.2018.05.045>
- J.D.C. Carregosa, J.P.F. Grilo, G.S. Godoi, D.A. Macedo, R.M. Nascimento, R.M.P.B. Oliveira, Microwave-assisted hydrothermal synthesis of ceria (CeO₂): microstructure, sinterability and electrical properties. *Ceram. Internat.* **46**, 23271–23275 (2020). <https://doi.org/10.1016/j.ceramint.2020.06.021>
- Y. Tao, F.H. Gong, H. Wang, G.L. Tao, Microwave-assisted preparation of cerium dioxide nanocubes. *Mater. Chem. Phys.* **2008112**(3), 973–976 (2008). <https://doi.org/10.1016/j.matchemphys.2008.07.018>
- H. Yang, C. Huang, A. Tang et al., Microwave-assisted synthesis of ceria nanoparticles. *Mat. Res. Bull.* **40**, 1690–1695 (2005). <https://doi.org/10.1016/j.jmrt.2021.04.036>
- V.P. Pakharukova, É.M. Moroz, D.A. Zyuzin, Construction of the model radial distribution curves with regard to the features of x-ray diffraction experiment. *J. Struct. Chem.* **51**, 274–280 (2010). <https://doi.org/10.1007/s10947-010-0042-y>
- D.A. Zyuzin, E.M. Moroz, A.S. Ivanova, A.N. Shmakov, G.N. Kustova, Local structure of amorphous and highly dispersed zirconium hydroxides and oxides. *Kinet. Catal.* **45**, 739–742 (2004). <https://doi.org/10.1023/B:KICA.0000044988.66511.2d>
- The thermal decomposition of lanthanum hydroxide [Electronic resource], Chemiday.com. 2015. <https://chemiday.com/reaction>
- D.J. Kim, Lattice parameters, ionic conductivities, and solubility limits in fluorite-structure MO₂ oxide [M = Hf⁴⁺, Zr⁴⁺, Ce⁴⁺, Th⁴⁺, U⁴⁺] solid solutions. *J. Am. Ceram. Soc.* **72**, 1415–1421 (1989). <https://doi.org/10.1111/j.1151-2916.1989.tb07663.x>
- S. Zec, S. Boskovic, B. Kalurerovic et al., Chemical reduction of nanocrystalline CeO₂. *Ceram. Int.* **35**, 195–198 (2009). <https://doi.org/10.1016/j.ceramint.2007.10.031>
- D.N. Durgasri, T. Vinodkumar, P. Sudarsanam, B.M. Reddy, Nanosized CeO₂–Gd₂O₃ mixed oxides: study of structural characterization and catalytic CO oxidation activity. *Catal. Lett.* **144**(6), 971–979 (2014). <https://doi.org/10.1007/s10562-014-1223-7>
- Z.D. Dohčević-Mitrović, M.J. Šćepanović, M.U. Grujić-Brojčin, Z.V. Popović, S.B. Bošković, B.M. Matović, M.V. Zinkevich, F. Aldinger, The size and strain effects on the Raman spectra of Ce_{1-x}Nd_xO_{2-δ} (0 ≤ x ≤ 0.25) nanopowders. *Solid State Commun.* **137**(7), 387–390 (2006). <https://doi.org/10.1016/j.ssc.2005.12.006>
- F. Meng, Z. Fan, C. Zhang, Y. Hu, T. Guan, A. Li, Morphology-controlled synthesis of CeO₂ microstructures and their room temperature ferromagnetism. *J. Mater. Sci. Technol.* **33**(5), 444–451 (2017). <https://doi.org/10.1016/j.jmst.2016.06.018>
- NIST Chemistry WebBook <https://webbook.nist.gov/cgi/cbook.cgi?Formula=NO2&NoIon=on&Units=SI&cMS=on#Mass-Spec>
- S. Smart, S. Liu, J.M. Serra, J.C. Diniz da Costa, A. Iulianelli, A. Basile, Porous ceramic membranes for membrane reactors. *Handbook Membr. React.* **1**, 298–336 (2013). <https://doi.org/10.1533/9780857097330.2.298>
- J. Choma, M. Kloske, M. Jaroniec, An improved methodology for adsorption characterization of unmodified and modified silica gels. *J. Colloid Interface Sci.* **266**, 168–174 (2003). [https://doi.org/10.1016/S0021-9797\(03\)00573-3](https://doi.org/10.1016/S0021-9797(03)00573-3)
- C. Weidenthaler, Pitfalls in the characterization of nanoporous and nanosized materials. *Nanoscale* **3**, 792–810 (2011). <https://doi.org/10.1039/c0nr00561d>
- C. Binet, M. Daturi, J.C. Lavalley, IR study of polycrystalline ceria properties in oxidised and reduced states. *Catal. Today* **50**(2), 207–225 (1999). [https://doi.org/10.1016/S0920-5861\(98\)00504-5](https://doi.org/10.1016/S0920-5861(98)00504-5)
- L. Bin, L. Congming, Z.H. Guoqiang, Y. Xuesi, Oxygen vacancy promoting dimethyl carbonate synthesis from CO₂ and methanol over Zr-doped CeO₂ nanorods. *ACS Catal.* **8**, 10446–10456 (2018). <https://doi.org/10.1021/acscatal.8b00415>

Publisher's Note Springer Nature remains neutral with regard to jurisdictional claims in published maps and institutional affiliations.

Springer Nature or its licensor (e.g. a society or other partner) holds exclusive rights to this article under a publishing agreement with the

author(s) or other rightsholder(s); author self-archiving of the accepted manuscript version of this article is solely governed by the terms of such publishing agreement and applicable law.